Metasurface Absorber-Emitter for Humidity Sensing

Zhilu Ye, Minye Yang, and Pai-Yen Chen

Abstract – Accurate measurement of relative humidity is important in applications involving moisture-sensitive processes, such as epitaxy and allylation reactions. We propose here a humidity sensor based on parity-time-symmetric optical metasurfaces operating at the self-dual spectral singularity—the coherent perfect absorber-laser point. We theoretically study the performance and detection limit of this metasurface-based optical humidity sensor. Our results show that the sensitivity and resolution can be greatly enhanced at the coherent perfect absorber-laser point, with a modulation depth over 40 dB for relative humidity rising from 0% to 100%. The proposed sensor may pave a promising route for realization of a rapid and high-precision remote tool for detecting air humidity.

1. Introduction

Humidity sensors, translating the amount of water vapor into a measurable parameter, have great significance in assorted industrial, agricultural, and meteorological applications [1–6]. These humidity sensors can be divided into three categories: those based on mechanical deflections [1, 2], thermal variations [3], and changes of electrical properties with humidity level [4–6]. Among these sensors, capacitive ones may be the most attractive, due to their compact size, low power consumption, and easy fabrication process. They typically consist of a moisture-sensitive dielectric slab sandwiched by two conductive electrodes, and thus the capacitance can respond to alterations of the dielectric constant caused by moisture absorption and release. Despite the advantages of capacitive humidity sensors, they exhibit only moderate sensitivity and detection limits. In most reported works, the capacitance increases a few or tens of picofarads when relative humidity (RH) grows from 0% to 100% [6–8], or the capacitance variation when RH increases from 0% to 20% is inconspicuous [5, 9]. Such sensing performance is obviously insufficient to support application scenarios where there are highly strict requirements on humidity conditions—for example, detection of moisture during cellular and biochemical analysis [10], cryogenic processes [11], and semiconductor manufacturing and packaging [12]. It is therefore imperative to develop an ultrasensitive humidity sensor which can respond sensitively to tiny changes in the moisture level.

Manuscript received 24 December 2021.

Zhilu Ye, Minye Yang, and Pai-Yen Chen are with the Department of Electrical and Computer Engineering, University of Illinois at Chicago, Chicago, Illinois 60607, USA; e-mail: zye27@uic.edu, myang66@uic.edu, pychen@uic.edu.

In this work, we propose a humidity-sensing system based on the coherent perfect absorber-laser (CPAL) effect of parity-time (PT)-symmetric non-Hermitian metasurfaces (Figure 1a). PT-symmetric non-Hermitian Hamiltonians have attracted growing interest ever since their discovery. Particularly, PT-symmetry-enabled singularities such as exceptional points and CPAL points have found a number of applications in optical and electromagnetic systems [13–17] and wireless sensor telemetry [18–22]. As shown in Figure 1a, the PT-symmetric CPAL humidity sensor is formed by a pair of active and passive metasurfaces and a moisture-sensitive dielectric slab closely between them. The PT-symmetric humidity sensor is initially kept at the CPAL point, which indicates the coexistence of a CPA state (i.e., fully absorbing incident waves) and a lasing state (i.e., extreme irradiance) at a fixed operating frequency. Variation in RH may affect the dielectric constant or relative permittivity of the dielectric material, giving rise to dramatic change in eigenvalues/eigenstates and output signals of the system. Our systematic analysis shows that the proposed PT-symmetric humidity sensor can outperform current state-of-the-art techniques with unprecedented sensitivity and an enhanced detection limit. This endows it with great potential in precise monitoring and control of moisture conditions and detection of environmental properties.

2. Configuration and Results

Figures 1a–b show the schematic and equivalent transmission line model of the proposed optical humidity sensors formed by PT-symmetric metasurfaces. The active and passive metasurfaces (i.e., gain and loss components with surface conductances of $-G$ and G) can be practically realized with active optical metasurfaces (e.g., optically pumped two-dimensional nanostructures [23, 24]) and resistive metal sheets, respectively. The dielectric material between the metasurfaces has a thickness of d and a relative permittivity of ε_1 (under the dry condition, RH = 0%). When the RH increases, moisture absorption makes the dielectric material become a mixture of the original material and water with dielectric constant of ε ($\varepsilon = \varepsilon_1 + \Delta\varepsilon$). This dielectric mixture can be equivalent to a transmission line with an electrical length of $x = \beta d = \beta(d_0 + \Delta d)$ and a characteristic admittance of $Y = \sqrt{\varepsilon/\varepsilon_0}Y_0$, where $\beta = \omega\sqrt{\mu\varepsilon}$ is the propagation constant, d_0 is the ideal dielectric thickness leading to the CPAL point, Δd is an offset of physical length, ω is the angular operating frequency, $Y_0 = \sqrt{\varepsilon_0/\mu_0}$ is the intrinsic admittance of the air, and $\varepsilon(\mu)$ and $\varepsilon_0(\mu_0)$ are

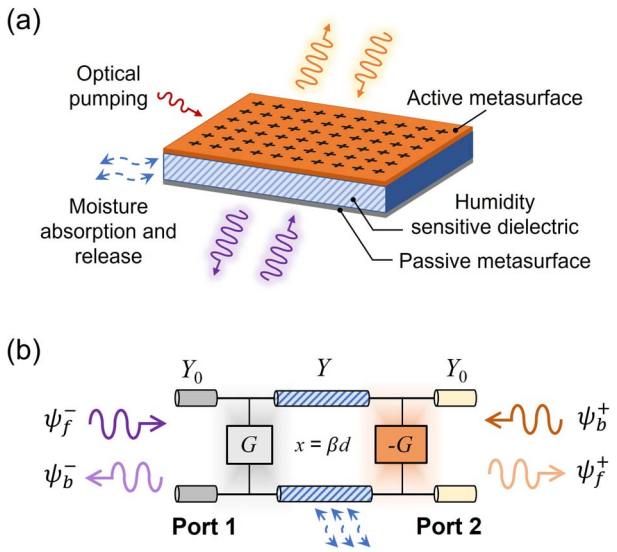

Figure 1. (a) Schematics and (b) equivalent transmission line model of the proposed parity-time-symmetric coherent perfect absorber-laser humidity sensor. The dielectric material with permittivity sensitive to humidity is sandwiched between the active and passive metasurfaces.

the relative permittivities (permeabilities) of the dielectric mixture and the air, respectively. The permeability of the dielectric material μ is insensitive to the humidity level, since water's permeability is nearly equivalent to that of the air.

The incoming and outgoing lights of the two-port transmission line network in Figure 1b can be related by the scattering matrix: $\left(\psi_f^+, \psi_b^-\right)^{\mathrm{T}} = \mathbf{S}\left(\psi_f^-, \psi_b^+\right)^{\mathrm{T}}$, where $\psi_f^{\pm}$ and $\psi_b^{\pm}$ denote the amplitudes of forward- and backward-propagating light waves. Figure 2a plots the evolution of the eigenvalues ($|\lambda_{\pm}|$) of the scattering matrix $\mathbf{S}$ with the gain-loss parameter $\gamma = G/Y_0$ and the electrical length x. It can be seen that the CPAL point occurs when $\gamma = \sqrt{2}$ and $x = \pi/2$, where two eigenvalues diverge into zero (CPA state) and infinity (lasing state). To better describe the CPAL effect of PT-symmetric metasurfaces, we define the output coefficient Θ as the ratio of output power to input power of the system: $\Theta = \left(\left|\psi_b^-\right|^2 + \left|\psi_f^+\right|^2\right) \Big/ \left(\left|\psi_f^-\right|^2 + \left|\psi_b^+\right|^2\right)$. The output coefficient can be manipulated by adjusting the complex amplitude ratio of two incident light waves α $\left(\alpha = \psi_b^+ \big/ \psi_f^-\right)$. When $\alpha = i\left(\sqrt{2} - 1\right)$ and $\alpha = 0$, the output factor achieves the CPA and lasing modes, respectively, as seen in Figure 2b and [19–21]. For the proposed PT-symmetric humidity sensor, we initially make it reach the CPAL point at RH = 0%: $\gamma = \sqrt{2}$ and $\omega d_0 \sqrt{\mu\varepsilon_1} = \pi/2$. The output coefficient of the humidity sensor would be notably affected by increases in the humidity level, since it directly causes the increase of the dielectric constant and breaks the CPAL condition.

Figures 3a–b show the output coefficient of the PT-symmetric CPAL optical system as a function of the dielectric perturbation $v = \Delta\varepsilon/\varepsilon_1$ and the offset parameter $\sigma = \Delta d/d_0$, when the system is initially operating in CPA mode—that is, $\alpha = i\left(\sqrt{2} - 1\right)$—and lasing mode—that is, $\alpha = 0$. The output coefficient shown in Figure 3a can be approximated as

$$\Theta(v) \approx \frac{\pi^2 v^2}{64} + \mathrm{O}\left(v^3\right) \tag{1}$$

with a minimum value of $\min(\Theta_v) = \pi^2\sigma^2/16$. From Figure 3a, the CPAL-locked optical sensor is very sensitive to changes in the dielectric permittivity, which is tuned by changes in RH. The sensitivity or the slope of $\Theta(v^2)$ is determined by a factor of $\pi^2/64$ and is unrelated to σ. The value of σ does have an effect on the lower bound of Θ: reducing σ would cause a decrease of $\min(\Theta_v)$. Thus, the detection limit of the system, associated with lower bound of Θ, could theoretically approach infinitesimal when σ approaches zero. For the PT-symmetric sensor initially working at the lasing state, the output coefficient can be written as

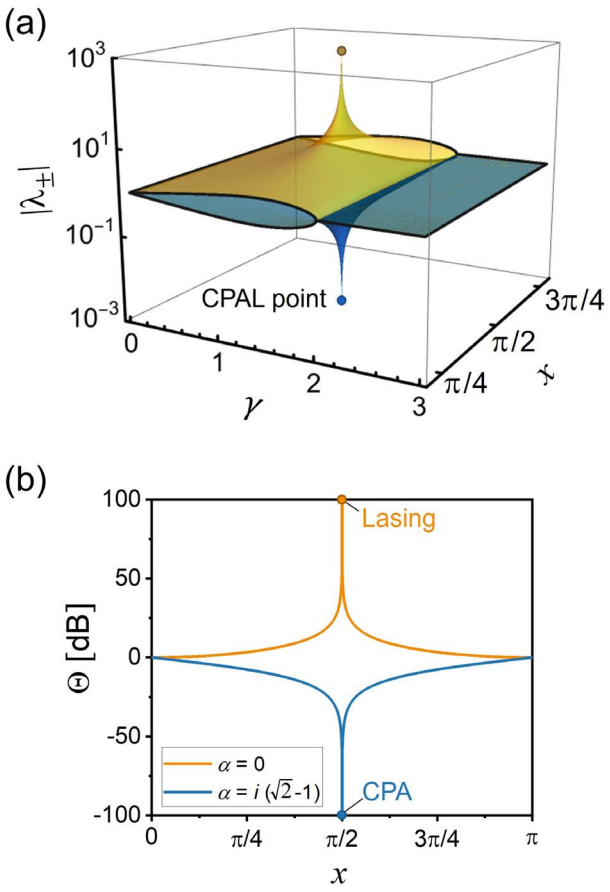

Figure 2. (a) Evolution of eigenvalues as a function of γ and x for the parity-time-symmetric humidity-sensing system in Figure 1. We note that a coherent perfect absorber-laser point occurs when $\gamma = \sqrt{2}$ and $x = \pi/2$. (b) Output coefficient versus electrical length x; here, $\gamma = \sqrt{2}$. At the coherent perfect absorber-laser point ($x = \pi/2$), the output coefficient becomes zero (coherent perfect absorber state) and infinity (lasing state), and is adjustable by the complex amplitude ratio between two input lights.

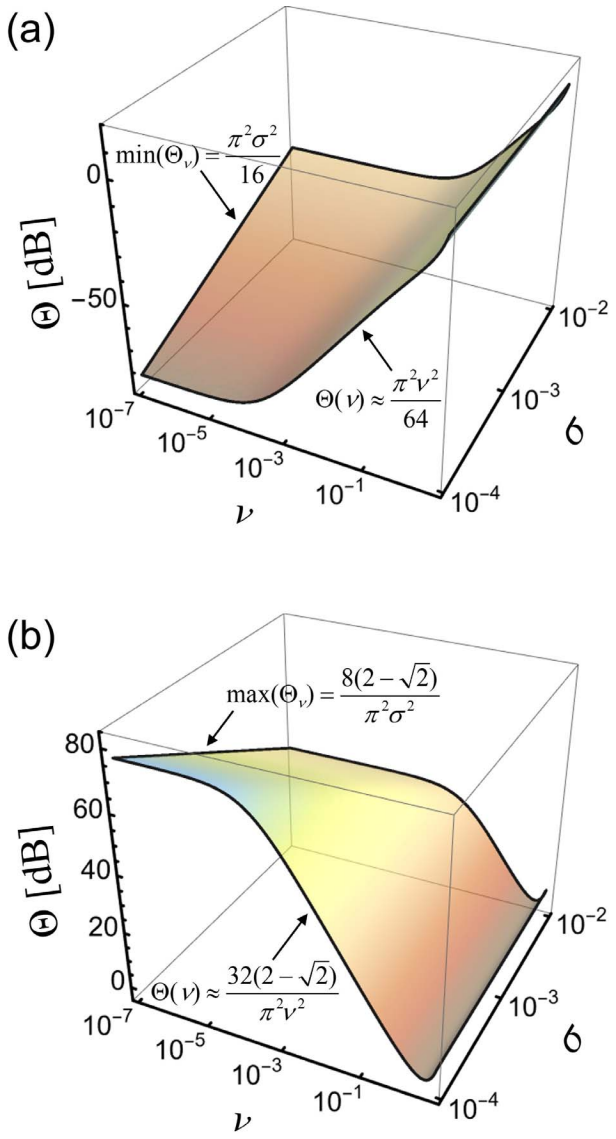

Figure 3. Output coefficient of the coherent perfect absorber-laser-locked optical humidity sensor operating in (a) the coherent perfect absorber state and (b) the lasing state. Here, $v = \Delta\varepsilon/\varepsilon_1$ is the perturbation on the dielectric constant and $\sigma = \Delta d/d_0$ is the offset parameter, related to the offset of electrical length.

$$\Theta(v) \approx \frac{32(2-\sqrt{2})}{\pi^2 v^2} + \mathrm{O}(v^3). \tag{2}$$

Equivalently, $\Theta(v^{-2})$ has a slope of $32(2-\sqrt{2})/\pi^2$, which is independent of σ. The output factor has an upper bound of $\max(\Theta_v) = 8(2-\sqrt{2})/\pi^2\sigma^2$, which approaches infinity when σ is close to zero. In addition, the influence of the offset σ on the detection range of the PT sensor may be suppressed by applying an appropriate scaling factor—that is, PT-reciprocal scaling symmetry [20]. The CPA operating mode requires low power intensity and thus ensures radiation safety. On the other hand, the lasing mode releases the restrictions on the careful control of complexed

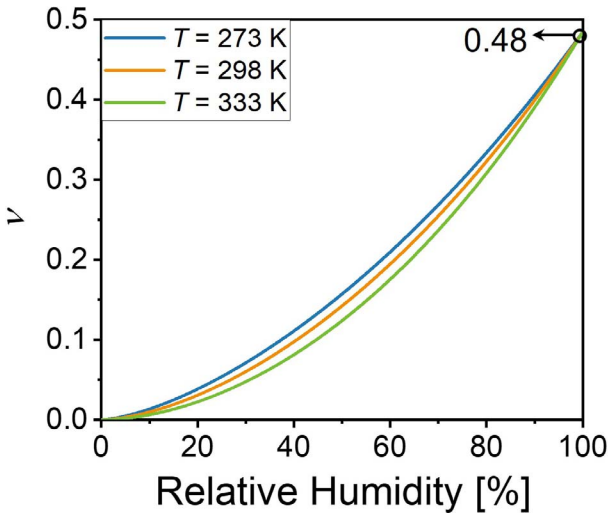

Figure 4. Dielectric perturbation $v = \Delta\varepsilon/\varepsilon_1$ vs. relative humidity at different ambient temperatures. For polyimide PIX-1400, v increases from 0 to 0.48 when relative humidity increases from 0% to 100%.

amplitude ratio between two incident lights, thereby simplifying experimental setups. Both CPA- and lasing-based sensing show extremely high sensitivity and enhanced detection limits, which are not possible with traditional capacitive humidity sensors that likewise monitor the change in the dielectric constant [5–9].

Various materials have been used for humidity sensing, such as metal oxides [4, 5], carbon nanotubes [25], and polymers [6–8]. Here, we take polyimide PIX-1400 (HD Microsystems, Hitachi, Japan) as an example to illustrate our CPAL-based optical humidity-sensor system, since it exhibits low hysteresis, high temperature stability, and biocompatibility. The dielectric constant of the polymer–water mixture can be calculated by Looyenga's equation [26]:

$$\varepsilon = \left(w\left(\varepsilon_2^{1/3} - \varepsilon_1^{1/3}\right) + \varepsilon_1^{1/3}\right)^3 \tag{3}$$

where w is the fractional volume of water absorbed, ε_2 is the dielectric constant of water, and ε_1, as already mentioned, is the dielectric constant of the polymer at RH = 0%. The volume of vapor absorbed and the environmental RH can be related by the Dubinin–Astakhov equation, which has been validated by numerous experiments [27, 28]:

$$w = w_m^0 \exp\left[-\left(\frac{RT\ln(p_s/p)}{E}\right)^n\right] \tag{4}$$

where w_m^0 is the maximum fractional volume of vapor absorbed at temperature $T_0 = 298$ K, R is the universal gas constant, T is the temperature in kelvins, E is the free energy of absorption, n is an empirical factor, and the ratio p_s/p of saturated vapor pressure to vapor pressure donates the reciprocal of relative humidity. Figure 4 plots the dielectric perturbation $v = \Delta\varepsilon/\varepsilon_1$ versus RH at different ambient temperatures T; here, for polyimide PIX-1400, $\varepsilon_1 = 2.93$, $\varepsilon_2 = 80$, $w_m^0 = 0.07$,

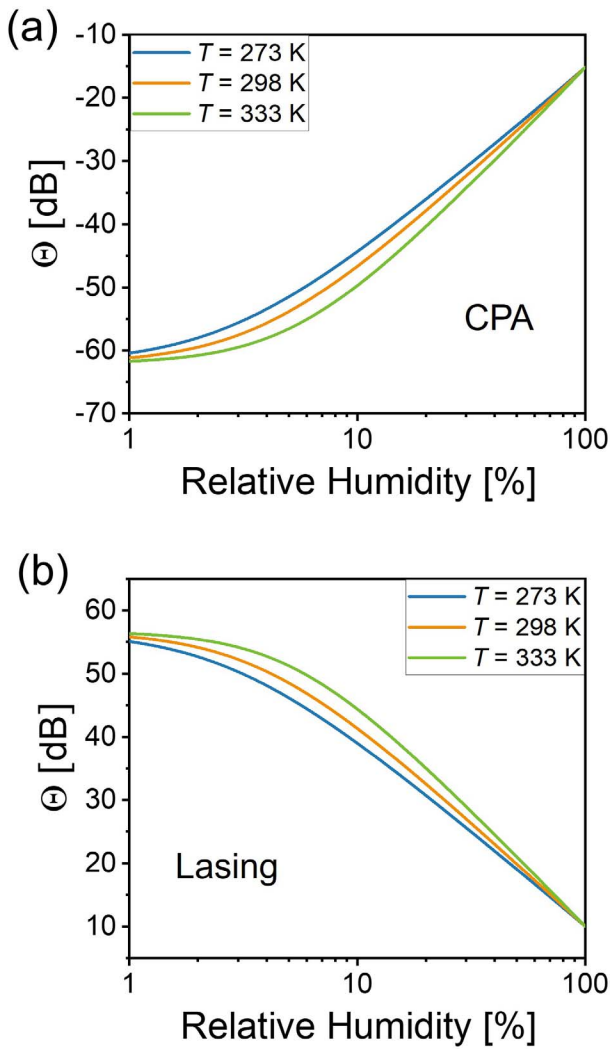

Figure 5. Output coefficient as a function of the relative humidity at different temperatures when the parity-time-symmetric coherent perfect absorber-laser humidity sensor initially operates in (a) the coherent perfect absorber state and (b) the lasing state. In both panels, $\sigma = \Delta d/d_0 = 10^{-3}$.

$E = 1516$ J, and $n = 1$. The dielectric perturbation v increases from 0 to 0.48 when the RH varies from 0% to 100%, corresponding to an increase in the dielectric constant from 2.93 to 4.35. This variation can result in remarkable changes in the output coefficients of the PT-symmetric humidity sensor, as shown in Figures 5a–b. The PT-symmetric humidity sensor exhibits preeminent sensitivity with various ambient temperatures ($T = 273$, 298, and 333 K) and different operating modes (CPA and lasing). The output coefficient varies by approximately 45 dB as RH changes from 0% to 100%. Particularly, the output variation is around 10 dB when RH increases from 0% to 10%, making the sensor suitable for monitoring small-scale alterations in moisture level. We note that the detection limit and working range of the proposed humidity sensor may be improved even further by suppressing σ or using PT-reciprocal scaling-symmetric topology.

Such sensing performance significantly surpasses that of conventional capacitive humidity sensors. In [6], with the same polymer but a traditional capacitive humidity-sensing scheme, a rise in RH from 0% to 100% can only lead to a capacitance change of approximately 1.3 pF. Even with advanced approaches (e.g., forming nanostructures on the surface of the polymer) to help enhance the sensing performance, the improvement is still limited—the capacitance variation is in tens of picofarads as the RH rises from 0% to 100%, or almost invisible when the RH is below 20% [5–9]. It is worth mentioning that although polyimide is discussed here for humidity sensing, the PT-symmetric CPAL humidity sensor may be integrated with many other materials (e.g., metal oxides [4, 5] and nano-materials [25]) whose dielectric constants are sensitive to moisture levels. In addition, the PT-symmetric humidity-sensing scheme may assimilate reported strategies such as, increasing the surface-to-volume ratio and optimizing the porosity of the material [6, 7], which may further improve its linearity, response and recovery times, and temperature stability.

3. Conclusion

We have proposed and theoretically studied a high-performance remote humidity sensor based on a PT-symmetric optical system formed by a pair of metasurfaces with balanced gain and loss. We have demonstrated that near the CPAL point, the sensor's output coefficient is highly sensitive to changes in relative humidity, with greatly enhanced sensitivity and detection limit compared with current humidity sensors. Further, the range of detection and sensitivity (slope of the output coefficient) are determined by the electrical (phase) distance $x = \pi/2 + \beta\Delta d$ between the two metasurfaces, and can be maximized by minimizing the phase offset $\beta\Delta d$. Our findings may lead the next-generation ultrasensitive remote humidity sensors for various industrial, instrumental, environmental, and high-end climate-control applications.

4. References

1. R. Buchhold, A. Nakladal, G. Gerlach, and P. Neumann, "Design Studies on Piezoresistive Humidity Sensors," *Sensors and Actuators B: Chemical*, **53**, 1–2, November 1998, pp. 1-7.
2. S. Chatzandroulis, A. Tserepi, D. Goustouridis, P. Normand, and D. Tsoukalas, "Fabrication of Single Crystal Si Cantilevers Using a Dry Release Process and Application in a Capacitive-Type Humidity Sensor," *Microelectronic Engineering*, **61–62**, July 2002, pp. 955-961.
3. T. M. Berlicki, E. Murawski, M. Muszyński, S. J. Osadnik, and E. L. Prociów, "Thermoelement Humidity Sensor," *Sensors and Actuators A: Physical*, **64**, 3, January 1998, pp. 213-217.
4. Y. Zhang, K. Yu, D. Jiang, Z. Zhu, H. Geng, et al., "Zinc Oxide Nanorod and Nanowire for Humidity Sensor,"

Applied Surface Science, **242**, 1–2, March 2005, pp. 212-217.
5. Y. Kim, B. Jung, H. Lee, H. Kim, K. Lee, et al., "Capacitive Humidity Sensor Design Based on Anodic Aluminum Oxide," *Sensors and Actuators B: Chemical*, **141**, 2, September 2009, pp. 441-446.
6. H. Lee, S. Lee, S. Jung, and J. Lee, "Nano-Grass Polyimide-Based Humidity Sensors," *Sensors and Actuators B: Chemical*, **154**, 1, May 2011, pp. 2-8.
7. W.-H. Zhou, L.-C. Wang, and L.-B. Wang, "Numerical Study of the Structural Parameter Effects on the Dynamic Characteristics of a Polyimide Film Micro-Capacitive Humidity Sensor," *IEEE Sensors Journal*, **16**, 15, August 2016, pp. 5979-5986.
8. P. J. Schubert and J. H. Nevin, "A Polyimide-Based Capacitive Humidity Sensor," *IEEE Transactions on Electron Devices*, **32**, 7, July 1985, pp. 1220-1223.
9. W. Chen, J. Huang, C. Zhu, F. Xu, and Q.-A. Huang, "An Interdigital Capacitive Humidity Sensor With Layered Black Phosphorus Flakes as a Sensing Material," *IEEE Sensors Journal*, **19**, 23, December 2019, pp. 11007-11013.
10. N. Jambunathan, J. M. Siani, and T. W. McNellis, "A Humidity-Sensitive *Arabidopsis* Copine Mutant Exhibits Precocious Cell Death and Increased Disease Resistance," *The Plant Cell*, **13**, 10, October 2001, pp. 2225-2240.
11. Y. Takayama and M. Nakasako, "Humidity-Controlled Preparation of Frozen-Hydrated Biological Samples for Cryogenic Coherent X-Ray Diffraction Microscopy," *Review of Scientific Instruments*, **83**, 5, May 2012, p. 054301.
12. J. H. Sohn, M. Atzeni, L. Zeller, and G. Pioggia, "Characterisation of Humidity Dependence of a Metal Oxide Semiconductor Sensor Array Using Partial Least Squares," *Sensors and Actuators B: Chemical*, **131**, 1, April 2008, pp. 230-235.
13. M. Yang, Z. Ye, M. Farhat, and P.-Y. Chen, "Cascaded PT-Symmetric Artificial Sheets: Multimodal Manipulation of Self-Dual Emitter-Absorber Singularities, and Unidirectional and Bidirectional Reflectionless Transparencies," *Journal of Physics D: Applied Physics*, **55**, 8, February 2022, p. 085301.
14. Z. Ye, M. Farhat, and P.-Y. Chen, "Tunability and Switching of Fano and Lorentz Resonances in *PTX*-Symmetric Electronic Systems," *Applied Physics Letters*, **117**, 3, July 2020, p. 031101.
15. R. El-Ganainy, K. G. Makris, M. Khajavikhan, Z. H. Musslimani, S. Rotter, et al., "Non-Hermitian Physics and PT Symmetry," *Nature Physics*, **14**, January 2018, pp. 11-19.
16. J. Doppler, A. A. Mailybaev, J. Böhm, U. Kuhl, A. Girschik, et al., "Dynamically Encircling an Exceptional Point for Asymmetric Mode Switching," *Nature*, **537**, September 2016, pp. 76-79.
17. Z. Ye, M. Yang, and P.-Y. Chen, "Multi-Band Parity-Time-Symmetric Wireless Power Transfer Systems," in *2021 IEEE Wireless Power Transfer Conference (WPTC)*, Jun. 2021, pp. 1-4. doi: 10.1109/WPTC51349.2021.9457925.
18. P.-Y. Chen, M. Sakhdari, M. Hajizadegan, Q. Cui, M. M.-C. Cheng, et al., "Generalized Parity-Time Symmetry Condition for Enhanced Sensor Telemetry," *Nature Electronics*, **1**, May 2018, pp. 297-304.
19. M. Yang, Z. Ye, M. Farhat, and P.-Y. Chen, "Enhanced Radio-Frequency Sensors Based on a Self-Dual Emitter-Absorber," *Physics Review Applied*, **15**, January 2021, p. 014026.
20. Z. Ye, M. Yang, L. Zhu, and P.-Y. Chen, "*PTX*-Symmetric Metasurfaces for Sensing Applications," *Frontiers of Optoelectronics*, **14**, 2, June 2021, pp. 211-220.
21. M. Farhat, M. Yang, Z. Ye, and P.-Y. Chen, "PT-Symmetric Absorber-Laser Enables Electromagnetic Sensors with Unprecedented Sensitivity," *ACS Photonics*, **7**, 8, August 2020, pp. 2080-2088.
22. M. Yang, Z. Ye, M. Farhat, and P.-Y. Chen, "Ultrarobust Wireless Interrogation for Sensors and Transducers: A Non-Hermitian Telemetry Technique," *IEEE Transactions on Instrumentation and Measurement*, **70**, August 2021, p. 1504709.
23. T. Low, P.-Y. Chen, and D. N. Basov, "Superluminal Plasmons With Resonant Gain in Population Inverted Bilayer Graphene," *Physical Review B*, **98**, 4, July 2018, p. 041403.
24. P.-Y. Chen and J. Jung, "PT Symmetry and Singularity-Enhanced Sensing Based on Photoexcited Graphene Metasurfaces," *Physical Review Applied*, **5**, 6, June 2016, p. 064018.
25. J. T. W. Yeow and J. P. M. She, "Carbon Nanotube-Enhanced Capillary Condensation for a Capacitive Humidity Sensor," *Nanotechnology*, **17**, 21, November 2006, pp. 5441-5448.
26. H. Looyenga, "Dielectric Constants of Heterogeneous Mixtures," *Physica*, **31**, 3, March 1965, pp. 401-406.
27. A. Gil and P. Grange, "Application of the Dubinin-Radushkevich and Dubinin-Astakhov Equations in the Characterization of Microporous Solids," *Colloids and Surfaces A: Physicochemical and Engineering Aspects*, **113**, 1–2, August 1996, pp. 39-50.
28. K. A. G. Amankwah and J. A. Schwarz, "A Modified Approach for Estimating Pseudo-Vapor Pressures in the Application of the Dubinin-Astakhov Equation," *Carbon*, **33**, 9, September 1995, pp. 1313-1319.